Scaling-relation based analysis of bifunctional catalysis: The case for homogeneous bimetallic alloys

Mie Andersen,*^{,†} Andrew J. Medford,^{‡,¶} Jens K. Nørskov,^{‡,¶} and Karsten Reuter^{†,‡,¶}

†Chair for Theoretical Chemistry and Catalysis Research Center, Technische Universität
München, Lichtenbergstr. 4, D-85747 Garching, Germany

‡SUNCAT Center for Interface Science and Catalysis, Department of Chemical
Engineering, Stanford University, Stanford, CA 94305, USA

¶SUNCAT Center for Interface Science and Catalysis, SLAC National Accelerator
Laboratory, 2575 Sand Hill Road, Menlo Park, CA 94025, USA

E-mail: mie.andersen@ch.tum.de

Abstract

We present a generic analysis of the implications of energetic scaling relations on the possibilities for bifunctional gains at homogeneous bimetallic alloy catalysts. Such catalysts exhibit a large number of interface sites, where second-order reaction steps can involve intermediates adsorbed at different active sites. Using different types of model reaction schemes, we show that such site-coupling reaction steps can provide bifunctional gains that allow for a bimetallic catalyst composed of two individually poor catalyst materials to approach the activity of the optimal mono-material catalyst. However, bifunctional gains can not result in activities higher than the activity peak of the monomaterial volcano curve as long as both sites obey similar scaling relations, as is generally the case for bimetallic catalysts. These scaling relation imposed limitations could be overcome by combining different classes of materials such as metals and oxides.

Keywords

bifunctional catalysis, computational chemistry, transition metals, bimetallic alloys, scaling relations

1 Introduction

Bifunctional catalysts, which combine the properties of two different active sites, have received considerable attention as a means to improve catalytic activities beyond the activities achievable with traditional monofunctional catalysts. 1-5 The properties of monofunctional transition metal (TM) catalysts have been subject to extensive theoretical studies over the last decades. Owing to the discovery of trends in the binding strengths of reaction intermediates over the TM series (i.e. scaling relations) enormous progress in the theoretical understanding of catalysis has been possible. 6-13 The trends over the TM series can, for example, be quantified as Brønsted-Evans-Polanyi (BEP) relationships that relate activation barriers to thermochemical reaction energies, or as thermochemical scaling relations that relate the adsorption strengths of reaction intermediates to each

other. This progress has enabled a quantitative understanding of the Sabatier principle, which states that a high catalytic activity is obtained by catalysts that provide intermediate adsorption energies of reaction intermediates, where binding too strongly limits the catalytic activity by making it difficult to desorb the product species and, vice versa, binding too weakly makes the adsorption and activation of reactants difficult. In this respect it is thus an intriguing question whether the limitations posed by the resulting volcano curves on traditional monofunctional catalysts could be overcome by bifunctional catalysts, which could provide a greater flexibility in the adsorption energies by making use of two active sites.

A recent first-principles microkinetic study on CO methanation indeed reported certain bimetallic catalysts to exhibit activities beyond the activity peak of the monometallic volcano curve. 14 For the employed explicit reaction networks and active site models, it can, however, be difficult to disentangle the different contributions to the observed changes in catalytic activity. In particular, it is difficult to discern whether the gains arise as a result of a "truly bifunctional effect" (i.e. multiple coupled active sites in the kinetic model) or as a result of the binding characteristics of a single bimetallic active site (i.e. a more favorable BEP relation providing lower activation barriers at the bimetallic active site). A way to circumvent this ambiguity is to make use of simplified model reaction schemes and active site models in order to single out the most important general effects. We recently made use of this strategy to analyze the bifunctional activity gains achievable from the diffusional coupling of two active sites. 15 It was found that the universality of scaling relations between adsorption energies on TM surfaces largely prevents any improvements through bifunctionality. In the present work we extend our considerations to bifunctional catalysts where the two active sites are neighboring on an atomic scale. Our previous and present studies can thus be seen as two limiting cases of the distribution of the active sites, one limit being a complete spatial separation with negligible amount of interface sites 15 and the other

limit being the perfect mixing with a maximal number of interface sites (present case). The present case could be found in practice on homogeneous bimetallic (alloy) catalysts ^{4,5,16,17} or at the interface between metal nanoparticle and non-metal support. ^{2,3,18} In addition to diffusion between the sites, such bifunctional catalysts allow for a coupling arising from second-order reaction steps that involve two reaction intermediates adsorbed on different types of active sites.

When the two active sites obey the same BEP relations, our analysis reveals such sitecoupling reaction steps as an essential ingredient to reach catalytically relevant bifunctional gains. However, we show that the activities reached could also be obtained in a single-site (monofunctional) kinetic model. To clarify the use of the term "bifunctionality", we therefore propose a novel definition differentiating between (i) "energetic bifunctionality" (the activities achieved by the coupling of two active sites could equally well be obtained in a singlesite kinetic model employing the BEP relations obeyed by the bifunctional active site and the optimal single-site adsorption energies) and (ii) "kinetic bifunctionality" (the activities achievable are "truly bifunctional effects" which arise from the kinetic coupling of two active sites and could not be obtained in a single-site kinetic model).

2 Theory

2.1 Reaction models

We base our analysis on three generic reaction schemes, which each are rate-limited by one adsorption and one or two reaction-desorption steps. Scheme 1 considers a first-order adsorption step of a single adsorbate A onto an active site s, which is followed by a second-order reaction-desorption step.

$$\begin{array}{c} A(\mathbf{g}) + *_{\mathbf{s}} \Longrightarrow A_{\mathbf{s}} \\ 2A_{\mathbf{s}} \Longrightarrow 2*_{\mathbf{s}} + A_{2}(\mathbf{g}) \end{array}$$

Scheme 1: Describes e.g. the hydrogen evolution reaction.

Schemes 2 and 3 consider a second-order adsorption step leading to two reaction intermediates A and B at the surface. For scheme 2 the reaction-desorption steps of A and B are considered to be second order.

$$AB(g) + 2*_s \Longrightarrow A_s + B_s$$

$$2A_s \Longrightarrow 2*_s + A_2(g)$$

$$2B_s \Longrightarrow 2*_s + B_2(g)$$

Scheme 2: Describes e.g. NO decomposition.

For scheme 3 the reaction-desorption steps of A and B are instead considered to be first order.

$$\begin{array}{c} AB(\mathbf{g}) + 2 *_{\mathbf{s}} \Longrightarrow A_{\mathbf{s}} + B_{\mathbf{s}} \\ A_{\mathbf{s}} \Longrightarrow *_{\mathbf{s}} + A(\mathbf{g}) \\ B_{\mathbf{s}} \Longrightarrow *_{\mathbf{s}} + B(\mathbf{g}) \end{array}$$

Scheme 3: Describes e.g. CO methanation.

Table 1 illustrates possible mappings between these simple reaction schemes and real reactions. If A(g) represents a solvated proton and electron and $A_2(g)$ represents $H_2(g)$, scheme 1 directly describes the hydrogen evolution reaction (HER). Similarly, if AB(g) represents NO(g), $A_2(g)$ represents $N_2(g)$ and $B_2(g)$ represents $O_2(g)$, scheme 2 describes NO decomposition. However, under suitable assumptions concerning the rate-limiting steps, more complex reaction networks such as CO methanation can also be approximated by a simpler reaction scheme. In the mapping of scheme 3 to CO methanation several reaction steps, for instance the four hydrogenation steps required to form CH₄ from C, have been considered as one hypothetical reaction-desorption step. Such mappings of several reaction steps to one hypothetical step have been considered previously in the literature, 19 and are consistent with the "lumped kinetic model" approach that is commonly used in kinetic modeling.²⁰ It has also been shown that the trends over the TM series for the hypothetical one-step hydrogenation reaction of C, O, or N to form CH₄, H₂O, or NH₃, respectively, could indeed be described by a single, generic BEP relation. 19 This finding justifies our approach based on a single BEP relation for each reaction step in the reaction scheme (vide infra) also for the case of more complex reactions.

Scheme 3 can thus be seen as a simplified model for CO methanation, for which bifunctional gains have been reported in previous work. 14 The three schemes differ from each other in two important aspects; (i) the order of the reaction steps and (ii) the number of reaction intermediates (only A or both A and B). The comparison of scheme 1 and 3 enables assessment of the effect of going from one to two reaction intermediates with the concomitant increase from two to four degrees of freedom spanned by the adsorption energies of the reaction intermediates on the two sites of the bifunctional catalyst (vide infra). In addition, the comparison of scheme 2 and 3 allows analysis of the effect of going from reaction steps of both first and second order (scheme 3) to only reaction steps of second order (scheme 2). The conclusion of this comparison is that as long as a second-order step involving two different reaction intermediates A and B is included in the reaction scheme, the order of the remaining steps seems unimportant. The overall conclusions derived from our study are therefore expected to apply quite generally to various types of reaction models; thus, these conclusions are expected to have general implications for the concept of bifunctionality as a whole.

2.2 Microkinetic modeling

The approach described below is identical to the approach followed in our previous publication.¹⁵ It is repeated here for ease of reading.

The microkinetic models are solved at steady state in the mean-field approximation using the CatMAP software package.²¹ The rate equations for elementary processes $i \rightarrow j$ take the form

$$r_{i \to j} = \frac{k_{\rm B}T}{h} \exp\left(\frac{-\Delta G_{i \to j}^{\rm act}}{k_{\rm B}T}\right) \prod_{p_k \in p_i} p_k \prod_{\Theta_k \in \Theta_i} \Theta_k,$$
(1)

where $k_{\rm B}$ is the Boltzmann constant, T is the temperature, h is Planck's constant, $\Delta G_{i\to j}^{\rm act}$ is the activation free energy of the elementary process $i\to j$, p_k is the gas pressure of species k in the initial state i, and Θ_k the corresponding coverage. Without loss of generality, the results

Table 1: Examples of possible mappings between model and real reaction schemes. For the more complex reaction scheme 3 (CO methanation), several reaction steps have been considered as one hypothetical step as described in the text and H₂ is assumed to react directly from the gas phase. In Sec. S3 it is shown that the latter assumption does not influence the conclusions regarding the possibilities for bifunctional gains.

Reaction order	Reaction scheme	Example
	(1)	Hydrogen evolution reaction
1	$A(g) + *_s \Longrightarrow A_s$	$e^{-}(aq) + p^{+}(aq) + *_{s} \rightleftharpoons H_{s}$
2	$2A_s \rightleftharpoons A_2(g) + 2*_s$	$2H_s \rightleftharpoons H_2(g) + 2*_s$
	(2)	NO decomposition
2	$AB(g) + 2*_s \Longrightarrow A_s + B_s$	$NO(g) + 2*_s \Longrightarrow N_s + O_s$
2	$2A_s \Longrightarrow 2*_s + A_2(g)$	$2N_s \Longrightarrow 2*_s + N_2(g)$
2	$2B_s \Longrightarrow 2*_s + B_2(g)$	$2O_s \Longrightarrow 2*_s + O_2(g)$
	(3)	CO methanation
2	$AB(g) + 2*_s \Longrightarrow A_s + B_s$	$CO(g) + 2*_s \rightleftharpoons C_s + O_s$
1	$A_s \rightleftharpoons *_s + A(g)$	$C_s + 2H_2(g) \Longrightarrow *_s + CH_4(g)$
1	$B_s \Longrightarrow *_s + B(g)$	$O_s + H_2(g) \Longrightarrow *_s + H_2O(g)$

will specifically be presented for $T=500\,\mathrm{K}$ and gas pressures of 1 bar. The entropy parts of the activation free energies are then calculated using a typical gas-phase entropy of $0.002\,\mathrm{eV/K}$, and zero-point vibrational energies and vibrational entropies of intermediates are neglected.

The enthalpy parts of the activation free energies of individual reaction steps, $\Delta E_{i\rightarrow j}^{\rm act}$, are assumed to follow BEP relations of the form

$$E_{i \to j}^{\text{act}} = \alpha \cdot \Delta E_{i \to j} + \beta$$
 . (2)

The reaction energies, $\Delta E_{i\rightarrow j}$, depend on the gas-phase enthalpies, where we choose the references (i.e. an enthalpy of 0 eV) to A(g) and B(g) (scheme 1 and 3) and $A_2(g)$ and $B_2(g)$ (scheme 2). For scheme 1 the enthalpy of $A_2(g)$ is, again without loss of generality, fixed to $-2 \, \text{eV}$, which ensures that the overall reaction is downhill in free energy by 1 eV. For scheme 2 the enthalpy of AB(g) is set to the value representative for NO decomposition (0.905 eV) from Ref., 22 while for scheme 3 the enthalpy of AB(g) is set to 1 eV, ensuring that the overall reaction is downhill in free energy by 2 eV.

Owing to the use of BEP relations, reaction scheme 1 effectively has only one free parameter (or descriptor) that covers the entire dependence on the actual catalyst used, namely the adsorption energy of reaction intermediate A, E_s^A . In case of scheme 2 and 3, this dependence extends to two free parameters, E_s^A and the adsorption energy of reaction intermediate B, E_s^B . We consider a range between $-4 \,\mathrm{eV}$ (strongly exothermic adsorption) and $+4 \,\mathrm{eV}$ (strongly endothermic adsorption) for these parameters, such that plots of the turnover frequency (TOF) as a function of these adsorption energies will lead to the well-known volcano plots in the monofunctional case.

2.3 Bifunctional model

To describe a bifunctional catalyst we extend schemes 1-3 to two hypothetical site types s and t. In our previous work we considered a coupling of the two sites exclusively through diffusion of reaction intermediates, e.g.

$$A_s + *_t \Longrightarrow *_s + A_t$$
 (3)

In this case, there was no need to explicitly consider scheme 3, as it does not add to the individual results found for the first- and second-order reactions in schemes 1 and 2. In this work we now additionally consider a coupling of the two sites through second-order reaction steps like

$$AB(g) + *_s + *_t \Longrightarrow A_s + B_t$$
 . (4)

Such a coupling is only possible when the two sites s and t are immediately neighboring on the atomic scale and we will refer to such steps as site-coupling steps from now on.

For diffusional coupling we consider only the difference in adsorption energy between the two sites as a thermodynamic barrier for the diffusion step. Any resulting bifunctional gain is then an upper limit as compared to the situation with additional kinetic diffusion barriers. For the bifunctional model representing active sites that are neighboring on the atomic scale, we specifically consider a random spatial distribution of the two site types s and t and apply the corresponding normalization to the rate constants of individual reaction pathways (cf. Sec. S1). This bifunctional model could represent a homogeneous bimetallic catalyst as suggested in Refs.^{4,5}

We will assume that the two sites s and t follow identical BEP relations. This conveys the assumption that the two site types are of similar geometry, such that only electronic changes, e.g. charge transfer between the constituents or changes in bond length (the ligand effect 23,24), occur in the alloy. It has been shown that the effect of the electronic changes in alloys on the adsorption energies of reaction intermediates can be predicted by the position and shape of the d-band.²⁵ The latter is the physical origin of the observed trends over the TM series quantified by the scaling relations. Correspondingly, alloys and pure metals have indeed been validated to follow the same BEP relations for several reactions. 26-28

The plausibility of bifunctional activity gains through both kinds of coupling is assessed in two ways: i) a gain relative to the sum of the activities of the two considered decoupled catalysts (hereafter denoted as relative bifunctional gain) and ii) a gain relative to the activity of two sites on the optimal monofunctional catalyst (hereafter denoted as absolute bifunctional gain).

3 Results

We begin by addressing reaction scheme 1 and BEP parameters representative for the HER on metal(111) facets from Ref. 29 Fig. 1 shows the resulting TOF maps for (a) coupling by diffusion only, 15 which represents spatially separated active sites, and (b) coupling by additionally allowing for site-coupling reaction steps, which represents active sites that are homogeneously distributed on the atomic scale. The decoupled TOF maps (center left plots) are, of course, identical for the two cases. Considering the variation of the TOF with H adsorption on one site, while keeping the H adsorption energy on the other site fixed, leads to the familiar one-dimensional (1D) volcano plots (each appearing as a stripe in 2D). These volcano plots are identical for the s and the t site, which is a mere consequence of the assumption of identical BEP parameters on the two sites. The 1D volcano plots illustrate the Sabatier principle quantified by the BEP relations, where the optimum catalytic activity is found for an intermediate adsorption energy of H.

The relative bifunctional gain is defined as the ratio of the coupled to the decoupled TOF and is quantified in the center right plots. For diffusional coupling (cf. Fig. 1(a)) only a tiny relative bifunctional gain at the descriptor point marked with an X is observed (see also the identical symmetrically related gain on the opposite side of the diagonal, which is not hidden by the X). The inclusion of site-coupling reaction steps allows instead for much larger relative gains (cf. Fig. 1(b)). It should be noted, though, that the observed gains would be of insignificant practical catalytic relevance, since the best obtained TOFs in the coupled case are still many orders of magnitude lower than the TOF of the optimal monofunctional (decoupled) catalyst. The greater relative bifunctional gains observed in Fig. 1(b) can be explained from the free energy diagrams for the descriptor points marked with an X (right plots), where the relative bifunctional gains arise from the coupled pathways marked with dashed black lines. In contrast to diffusional coupling only, the inclusion of sitecoupling reaction steps allows for the advanta-

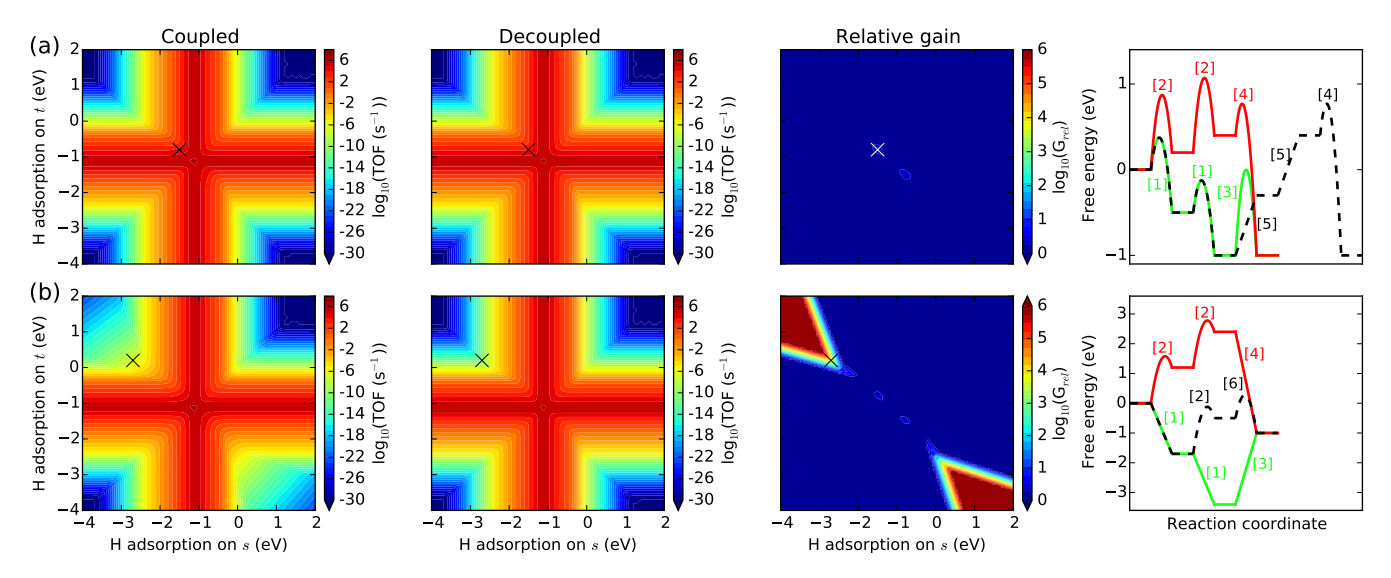


Figure 1: TOF maps for the model representing the HER on a (111) metal facet (scheme 1, BEP parameters from Ref.²⁹) for the bifunctionally coupled (left) and decoupled (center left) model, the relative bifunctional gain, G_{rel} (center right), defined as the ratio of the coupled to the uncoupled TOF, as well as the free energy diagram for the point marked with an X in the TOF maps (right). Contrasted are (a) coupling by diffusion only and (b) additional coupling by site-coupling reaction steps. The free energy diagram shows the decoupled pathways on the reactive s site (green solid line), on the noble t site (red solid line) and the coupled pathway (black dashed line) responsible for the bifunctional gain. The numbers refer to the individual reaction steps: 1 (2) H adsorption on the s (t) site, 3 (4) H_2 desorption from the s (t) site, 5 diffusion of H from s to t site, 6 site-coupling reaction of H on s site and H on t site to desorb as H_2 .

geous H_2 desorption step involving a strongly bound H atom at the more reactive s site and a weakly bound H atom at the more noble t site, instead of either two strongly bound H atoms (green pathway, s site exclusively) or two weakly bound H atoms (red pathway, t site exclusively). As discussed in Sec. S2 and illustrated in Fig. S1, identical conclusions can be made when instead considering a more representative temperature for electrochemical hydrogen evolution of $T = 300 \,\mathrm{K}$.

Next, we move to reaction scheme 2 and BEP parameters representative for NO decomposition on a (111) metal facet from Ref. ²² As before we contrast in Fig. 2 the TOF maps for (a) coupling by diffusion only and (b) coupling by additionally allowing for site-coupling reaction steps. For scheme 2 the adsorption energies of the two intermediates A and B on the two sites of the bifunctional catalyst span four dimensions, which makes it impossible to visualize all degrees of freedom in a 2D plot. In Fig. 2 we have chosen the adsorption energies of N and

O on the s site as descriptors, while the adsorption energies on the t site are fixed to the values representative for Ag. For the bifunctional catalyst coupled by diffusion only (cf. Fig. 2(a)), relative gains are again possible, but as for scheme 1 the TOFs achieved in the coupled case are always many orders of magnitude lower than the TOF of the optimal monofunctional catalyst. These relative gains are therefore not of practical catalytic relevance, consistent with the conclusions of Ref. ¹⁵

For the bifunctional catalyst additionally coupled by site-coupling reaction steps (cf. Fig. 2(b)), much more relevant gains are possible. The combination of the descriptor point representing Ag on the t site with the descriptor point representing the hypothetical metal marked with an X on the s site allows for a relative bifunctional gain that makes the coupled TOF approach the TOF of the optimal monofuntional catalyst. It thus becomes possible to combine two active sites that each have very poor catalytic properties to achieve a bifuncti-

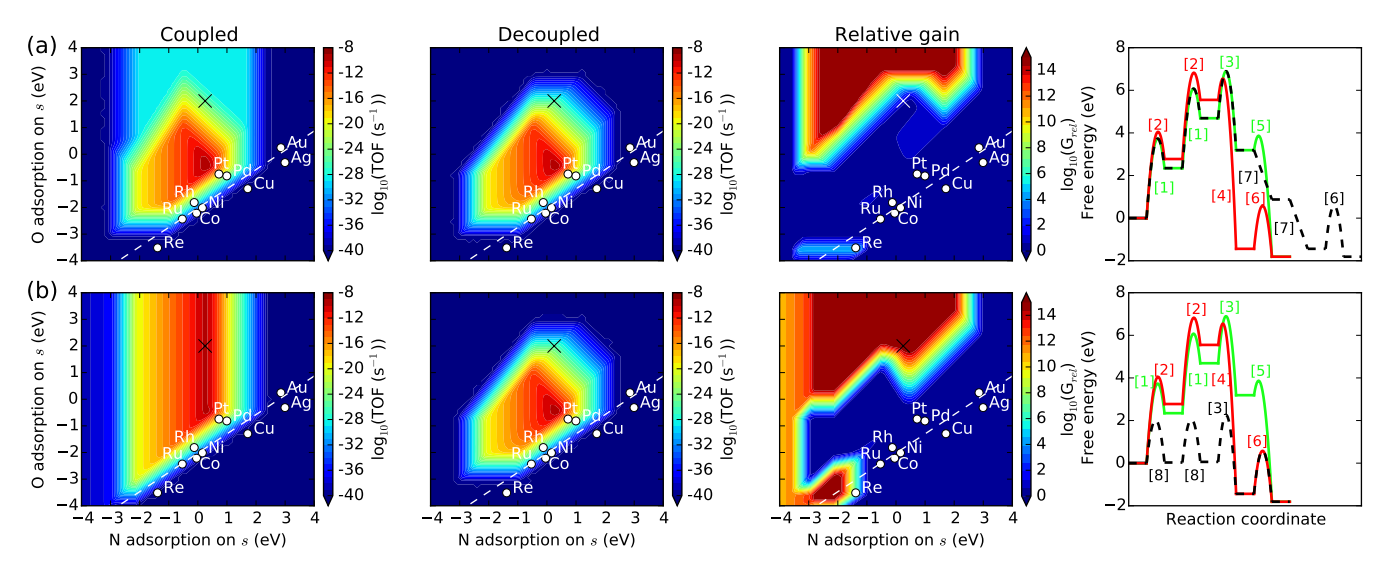


Figure 2: As Fig. 1, but for the model representing NO decomposition on a (111) metal facet (scheme 2, BEP parameters from Ref. 22). For the adsorption energies on the t site the values representative for Ag are used. Contrasted are (a) coupling by diffusion only and (b) additional coupling by site-coupling reaction steps. The numbers in the free energy diagrams refer to: 1 (2) NO dissociation on the hypothetical metal marked with an X in the TOF maps (on Ag), 3 (4) N₂ desorption from X (from Ag), 5 (6) O₂ desorption from X (from Ag), 7 diffusion of O from X to Ag, 8 site-coupling dissociation of NO with N adsorbing on X and O adsorbing on Ag. The dashed white line in the TOF maps is a linear fit to the descriptor points representing the elemental metals (see text).

onal catalyst that is as active as the optimal monofunctional catalyst. The reason for this behavior is clearly seen in the free energy diagrams (right plots): The bifunctional catalyst in Fig. 2(b) employs the site-coupling reaction step for NO adsorption, where N adsorbs on the s site (hypothetical metal X) and O adsorbs on the t site (Ag). Since the X descriptor point is located near the optimal N adsorption energy, while Ag is located near the optimal O adsorption energy, the bifunctional catalyst effectively employs optimal adsorption energies of N and O similar to the adsorption energies employed by the optimal monofunctional catalyst. This situation avoids high barriers for the adsorption and the desorption steps and leads to a TOF comparable to the optimal monofunctional catalyst.

The comparison of reaction scheme 1 and 2 up to this point has revealed that much greater possibilities for catalytically relevant bifunctional gains are found in scheme 2 as compared to scheme 1. The question thus naturally arises, whether these differences are caused by (i) the

larger number of second-order reaction steps in scheme 2, which could increase the possibilities of benefiting from site-coupling reactions steps, or (ii) the larger flexibility in the adsorption energies in scheme 2, which contains two reaction intermediates A and B instead of only A. In order to disentangle these two effects, we next consider reaction scheme 3 and BEP parameters representative for the simplified model for CO methanation from Ref. 19 discussed in Sec. 2.1. Note that scheme 1 is the reverse of scheme 3 for the case when the two intermediates A and B are identical, and that scheme 1 and 3 therefore contain the same number of second-order reaction steps, implying that differences between the two models arise from the fact that scheme 3 includes two different intermediates.

The results for scheme 3 are shown in Fig. 3, where we have chosen the adsorption energies of C and O on the s site as descriptors, while the adsorption energies on the t site are fixed to the values represented by the white dot marked Y. Similar to the conclusions reached for

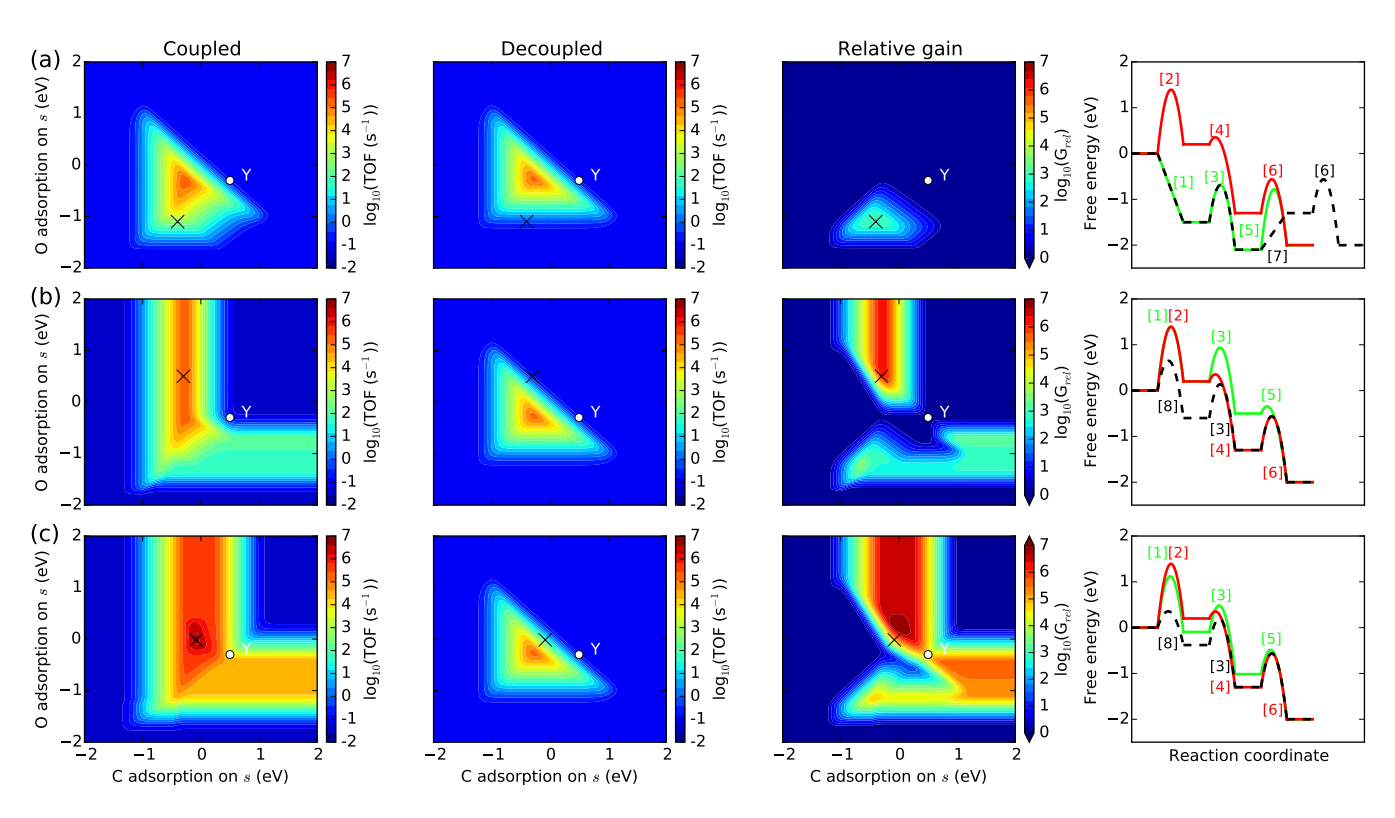


Figure 3: As Fig. 1, but for a simplified model for CO methanation on a stepped metal surface (scheme 3, BEP parameters from Ref. 19). For the adsorption energies on the t site the values marked with a white Y in the TOF maps are used. Contrasted are (a) coupling by diffusion only and (b) additional coupling by site-coupling reaction steps. In (c) the effect of decreasing the offset of the BEP relation for the site-coupling dissociation of CO by 0.5 eV is shown. The numbers in the free energy diagrams refer to: 1 (2) CO dissociation on the hypothetical metal marked with an X(Y) in the TOF maps, 3 (4) CH₄ reaction-desorption from X (from Y), 5 (6) H₂O reaction-desorption from X (from Y), 7 diffusion of O from X to Y, 8 site-coupling dissociation of CO with C adsorbing on X and O adsorbing on Y.

scheme 2, it is seen that the inclusion of sitecoupling reaction steps allows for the coupling of two active sites that individually exhibit poor activities (white dot Y and black X) to reach activities that are as high as for the optimal monofunctional catalyst. The important difference between scheme 1 and 2 is thus not related to the order of the involved reaction steps, but to the greater flexibility in adsorption energies when the reaction scheme includes two reaction intermediates instead of only one. Since the mapping of scheme 3 to CO methanation involves the approximation that hydrogen reacts directly from the gas phase, we repeat the analysis without this approximation in Sec. S3, reaching the same conclusions.

Finally, we comment upon the choice of the adsorption energies on the t site in Fig. 2 and Fig. 3. These descriptor points have been chosen to illustrate the possibilities of relative bifunctional gains in the best case, where one of the two adsorption energies on the t site (e.g. the O adsorption energy in scheme 2) corresponds to the optimal adsorption energy of the monofunctional catalyst. Correspondingly, the maximum relative gains arise when the other adsorption energy on the s site (e.g. the N adsorption energy in scheme 2) also corresponds to the optimal adsorption energy of the monofunctional catalyst. However, this only works for a choice of adsorption energies on the t site corresponding to the optimal monofunctional value for one species and a value that is higher (more endothermic adsorption) than the optimal value for the other species. As discussed in Sec. S4 and illustrated in Fig. S3, the bifunctional gains achievable through site-coupling reaction steps vanish when instead choosing adsorption energies on the t site corresponding to the optimal monofunctional value for one species and a value that is lower (more exothermic adsorption) than the optimal value for the other species.

4 A critical perspective

It is important to stress that our approach based on simple reaction schemes seeks to define

trends, rules, and limitations rather than making concrete predictions regarding the activities of specific bifunctional catalysts. Considering the results presented for scheme 2 in Fig. 2, one should note that it seems unlikely that the hypothetical metal X, for which we predict the largest bifunctional gains, really exists. When further inspecting the descriptor points representing the elemental TMs in Fig. 2, it is indeed observed that they obey a scaling relation between the adsorption energies of N and O (white dashed line). To this relation, point X would be an unrealistic outlier. In comparison, the scaling between C and O adsorption energies on TMs is less pronounced. 30 Thus, reactions involving these species might benefit from a greater flexibility in the adsorption energies and from the resulting lesser limitations to the extent of the 4D descriptor space open for exploration by the combination of promising elemental metals. Notwithstanding, when forming an alloy between two metals, the catalytic properties of the alloy constituents are generally affected by the electronic changes in the alloy. This could alter the adsorption energies as compared to the pure metal values that have been used in Fig. 2 to illustrate the general effect. While thus not meant to provide insight into bifunctional gains achievable by specific systems, the essential message of our study is that homogeneous bimetallic alloys should be much better candidates for efficient bifunctional catalysts than segregated bimetallic catalysts with only a low number of interface sites and a coupling that would predominantly be a result of diffusion.

However, it is also important to stress that the predicted achievable bifunctional gains are even for the case of site-coupling reactions still only relative. In other words, the activities of the bifunctional catalysts at no point in descriptor space exceed the activity of the optimal monofunctional catalyst. Performing a global search in the entire descriptor and BEP parameter space for both reaction scheme 1 and 2, cf. Sec. S5, we find this to hold true for any set of BEP parameters. This is not surprising, since the optimal monofunctional catalyst already employs optimum adsorption ener-

gies to take advantage of the best possible reaction pathway permitted by the BEP parameters for the reaction. We thus arrive at a rather limited perspective on bimetallic catalysts in the context of bifunctionality. This makes it imperative to distinguish between alloys that behave as a relatively homogeneous new metal and alloys that keep, or even enhance, the distinctive catalytic properties of the constituents. 24 The catalytic properties of the first type of alloys are an interpolation of those of the constituent metals. Of course, such interpolation aiming to reach the optimal monofunctional adsorption energies can and has already been successfully exploited even in commercial catalysts. 26-28,31-33 Yet, only the latter type of alloy, which provides two distinctive active sites, could be considered a bifunctional catalyst. From our analysis it is clear that the only mechanism by which such alloys can achieve a gain over catalysts made from pure metals is still only through the mixing of the properties of two metals in second-order reaction steps involving two different adsorbates A and B.

The maximal catalytic activity could thus just as well be captured in a single-site kinetic model employing the same BEP relations as the bifunctional kinetic model and the optimal single-site adsorption energies for A and B. This type of bifunctionality thus corresponds to our definition of "energetic bifunctionality" as discussed in the introduction. The specific difference between the well-known ligand effect and energetic bifunctionality is that the ligand effect is a "single-site" effect that occurs through ligand-induced changes to the electronic structure of a single active site, whereas bifunctional catalysts utilize two sites. When considering a second-order reaction step involving two adsorbates A and B, catalyst optimization through the ligand effect attempts to optimize the adsorption energies of both A and B at the single active site, whereas bifunctional catalysts attempt to optimize the adsorption energy of Aat one site type and the adsorption energy of Bat the other site type. The "energetic bifunctionality" concept thus allows for more flexibility in the adsorption energies. Specifically, every site is only required to have the optimal adsorption energy for one species (in contrast to both species simultaneously), which might be easier to achieve in practice.

Finally, we discuss how our results can be related to more detailed mechanistic studies on bimetallic catalysts such as the recent work on CO methanation over bimetallic catalysts ¹⁴ mentioned in the introduction. In Ref. 14 the active site model consists of a stepped surface, where the upper and lower step is made up of different metals A and B. This model thus offers the possibility for site-coupling reaction steps for e.g. CO dissociation, where one intermediate binds to metal A at the lower step and the other intermediate binds to metal B at the upper step. The finding that certain bimetallic catalysts, e.g. Ru-Re, Cu-Pt, and Cu-Re, can achieve activities higher than the optimal monofunctional catalyst (cf. Fig. 4 in Ref. 14) is thus at variance with our finding that absolute bifunctional gains are not possible. The most obvious explanation for this discrepancy is that the bimetallic catalysts explored in Ref. 14 do not fulfill the assumption made in our study that the alloys follow the same BEP relations as the pure TMs. Indeed, a closer inspection of the BEP relation for one of the rate-determining steps (CO dissociation, cf. Fig. 5(b) in Ref. 14), reveals that the bimetallic catalysts, for which activities higher than the optimal monofunctional catalyst were found, are outliers that seem to follow a BEP relation with the same slope but about 0.5 eV lower offset than the BEP relation followed by the elemental TMs. In order words, the barriers for CO dissociation for the alloys are consistently 0.5 eV lower than for the elemental TMs. In order to assess the general effect of such deviations from the BEP relations, we show in Fig. 3(c) the results for our simplified CO methanation model when employing a BEP relation with a 0.5 eV lower offset for site-coupling dissociation of CO as compared to the dissociation of CO exclusively occurring on s or t sites. As expected, the coupled catalyst can now achieve activities higher than the optimal monofunctional catalyst, i.e. an absolute bifunctional gain of the coupled catalyst over the decoupled catalyst can be found. However, the increased activity is not a result of "kinetic

bifunctionality" (cf. our definition in the introduction), since an equivalent activity is possible in a monofunctional model employing the BEP relations valid for the interface sites and the optimal single-site adsorption energies (cf. Sec. S6 and Fig. S4). The absolute bifunctional gain in Fig. 3(c) is about a factor of 30, which is comparable to the gains found in Ref. ¹⁴ The rather low absolute gain reflects the fact that not only the CO dissociation step, but all three reaction steps in the kinetic model, are rate-limiting near the top of the monofunctional volcano. Larger gains could be expected if also the other reaction steps in the kinetic model would follow more favorable BEP relations at the interface.

A further point to notice is that no attempt was made in Ref. 14 to assess the stability of the employed bimetallic catalysts. It is thus possible that the more favorable BEP relation followed by some of the bimetallic catalysts is caused by a poor or unstable atomic-scale model of the interface, since unstable active sites will in general be more reactive. On the other hand, it is well-known that BEP relations are not exact, and the search for favorable outliers has indeed been suggested as a possible catalyst discovery strategy.³⁴ Whereas the deviations from BEP relations found for TMs and their alloys are typically rather small, this might not necessarily be the case when combining different classes of materials such as metals and oxides. One could therefore imagine that enhanced possibilities for overcoming the limitations posed by the monofunctional (TM only) volcano curve could be found at interface sites between metal particles and oxide supports. Indeed, the favorable catalytic properties of such interface sites have already been discussed in the literature. 2,3,18

The combination of different classes of materials was also suggested in our previous work as a viable strategy for designing diffusionally coupled bifunctional catalysts. ¹⁵ Here we identified large absolute bifunctional gains when two active sites s and t follow different BEP relations that vary from each other in a way that makes one reaction step most favorable on one site type and another reaction step most favorable on the other site type. These gains could not be achieved in a single-site kinetic model and are

thus an example of "kinetic bifunctionality". In contrast, for the absolute gain found in the present work as a result of site-coupling reactions at interfaces, we showed that the same activity could be achieved in a single-site kinetic model, as long as the model employs the BEP relations valid for the interface sites. Such an interface site could thus just as well be considered an optimized monofunctional site in a single-site kinetic model and the gains achievable are thus a result of "energetic bifunctionality".

5 Conclusions

In conclusion, our analysis of homogeneous bimetallic catalysts has shown that much larger relative bifunctional gains can be achieved for sites that are neighboring on the atomic scale. Such sites provide for site-coupling second-order reaction steps, as compared to spatially separated active sites which only allow for coupling by diffusion. The way that homogeneous bimetallic alloys, which contain distinct, neighboring adsorption sites, reach activities approaching those of the optimal monofunctional catalyst is similar to the way alloys function, which provide a single adsorption site with adsorption energies interpolating those of the constituent metals. In essence, the deciding factor is the additional flexibility in the adsorption energies provided by both types of alloys, which in turn allows to approach the adsorption energies employed by the optimal monofunctional catalyst.

Our analysis has shown that the greatest possibilities for approaching optimal monofunctional activities for these homogeneous bimetallic alloys is obtained when the reaction scheme includes (at least) two reaction intermediates and a second-order rate-limiting reaction step involving an AB species as given in Eq. 4, whereas the order of the remaining reaction steps in the reaction scheme seems unimportant. In this case, large relative gains were found for bifunctional catalysts, where one site employs the optimal monofunctional adsorption energy for species A and a higher (more endothermic) adsorption energy for species B, while the ot-

her site employs the optimal monofunctional adsorption energy for species B and a higher (more endothermic) adsorption energy for species A. We observed, though, that in real systems the adsorption energies of the two species A and B could be related to each other through an approximate scaling relation. This could set limitations to the extent of descriptor space actually accessible by real alloys.

Using global optimization techniques, we have shown in general that no absolute bifunctional gains can be achieved as long as the alloys follow the same BEP relations as the pure metals. However, if interface sites following more favorable BEP relations could be identified, absolute gains resulting in activities higher than the peak of the monofunctional volcano curve could be expected. To identify such favorable interface sites, we generally suggest that the combination of different classes of materials such as oxides and metals will be a promising strategy to overcome the limitations posed by the BEP relations on TMs and their alloys. Such material combinations might also help to overcome the limitations posed by the approximate scaling relations identified between for instance N and O on TMs.

When the bifunctional gains arise from an interface site, whether or not this site obeys a more favorable BEP relation than the monofunctional sites, it can be expected that the activities achievable could also be captured in a single-site kinetic model making use of the BEP relation valid for the interface site and the optimal single-site adsorption energies. We have proposed the term "energetic bifunctionality" for such bifunctional gains. In contrast, we reserve the term "kinetic bifunctionality" to the cases where the bifunctional activities achievable can not be captured in a single-site kinetic model, such as the diffusional coupling of two sites following different BEP relations.

Supporting Information Available

Supporting Information. Normalization of rate constants, results for reaction scheme 1 at T=

300 K, more detailed reaction model for CO methanation, dependence of relative bifunctional gain on choice of descriptor points, global optimization, single-site kinetic model of an interface site obeying a more favorable BEP relation, CatMAP scripts used to generate the figures. This material is available free of charge via the Internet at http://pubs.acs.org.

Acknowledgement M.A. acknowledges funding from the Alexander von Humboldt foundation. A.J.M is grateful for support through the Department of Defense National Defense Science and Engineering Graduate Fellowship (NDSEG) program.

References

- (1) Nørskov, J. K.; Vojvodic, A. *Natl. Sci. Rev.* **2015**, 2, 140–149.
- (2) Saavedra, J.; Doan, H. A.; Pursell, C. J.; Grabow, L. C.; Chandler, B. D. *Science* **2014**, *345*, 1599–1602.
- (3) Germani, G.; Schuurman, Y. AIChE J. **2006**, 52, 1806–1813.
- (4) Kotobuki, M.; Watanabe, A.; Uchida, H.; Yamashita, H.; Watanabe, M. *J. Catal.* **2005**, *236*, 262–269.
- (5) Yajima, T.; Uchida, H.; Watanabe, M. *J. Phys. Chem. B* **2004**, *108*, 2654–2659.
- (6) Pallassana, V.; Neurock, M. *J. Catal.* **2000**, *191*, 301–317.
- (7) Nørskov, J. K.; Bligaard, T.; Logadottir, A.; Bahn, S.; Hansen, L. B.; Bollinger, M.; Bengaard, H.; Hammer, B.; Sljivancanin, Z.; Mavrikakis, M.; Xu, Y.; Dahl, S.; Jacobsen, C. J. H. J. Catal. **2002**, 209, 275–278.
- (8) Michaelides, A.; Liu, Z.-P.; Zhang, C. J.; Alavi, A.; King, D. A.; Hu, P. J. Am. Chem. Soc. **2003**, 125, 3704–3705.
- (9) Abild-Pedersen, F.; Greeley, J.; Studt, F.; Rossmeisl, J.; Munter, T. R.; Moses, P. G.;

- Skúlason, E.; Bligaard, T.; Nørskov, J. K. *Phys. Rev. Lett.* **2007**, *99*, 016105.
- (10) Nørskov, J. K.; Bligaard, T.; Hvolbæk, B.; Abild-Pedersen, F.; Chorkendorff, I.; Christensen, C. H. Chem. Soc. Rev. 2008, 37, 2163–2171.
- (11) Loffreda, D.; Delbecq, F.; Vigne, F.; Sautet, P. Angew. Chem. Int. Ed. 2009, 48, 8978–8980.
- (12) Calle-Vallejo, F.; Loffreda, D.; Koper, M. T. M.; Sautet, P. Nat. Chem. 2015, 7, 403–410.
- (13) Greeley, J. Annu. Rev. Chem. Biomol. Eng. **2016**, 7, 605–635.
- (14) Wang, Z.; Wang, H.-F.; Hu, P. *Chem. Sci.* **2015**, *6*, 5703–5711.
- (15) Andersen, M.; Medford, A. J.; Nørskov, J. K.; Reuter, K. Angew. Chem. Int. Ed. 2016, 55, 5210-5214.
- (16) Xu, B.; Siler, C. G. F.; Madix, R. J.; Friend, C. M. Chem. - Eur. J. 2014, 20, 4646–4652.
- (17) Lucci, F. R.; Marcinkowski, M. D.; Lawton, T. J.; Sykes, E. C. H. J. Phys. Chem. C 2015, 119, 24351–24357.
- (18) Vilhelmsen, L. B.; Hammer, B. ACS Catal. **2014**, 4, 1626–1631.
- (19) Cheng, J.; Hu, P.; Ellis, P.; French, S.; Kelly, G.; Lok, C. M. J. Phys. Chem. C 2008, 112, 1308-1311.
- (20) Deutschmann, O., Ed. Modeling and Simulation of Heterogeneous Catalytic Reactions: From the Molecular Process to the Technical System; Wiley-VCH Verlag & Co. KGaA, Boschstr. 12, 69469 Weinheim, Germany, 2011; pp 1–370.
- (21) Medford, A. J.; Shi, C.; Hoffmann, M. J.; Lausche, A. C.; Fitzgibbon, S. R.; Bligaard, T.; Nørskov, J. K. Catal. Lett. 2015, 145, 794–807.

- (22) Falsig, H.; Shen, J.; Khan, T. S.; Guo, W.; Jones, G.; Dahl, S.; Bligaard, T. *Top. Catal.* **2014**, *57*, 80–88.
- (23) Liu, P.; Nørskov, J. K. *Phys. Chem. Chem. Phys.* **2001**, *3*, 3814–3818.
- (24) Gross, A. Top. Catal. **2006**, 37, 29–39.
- (25) Xin, H.; Vojvodic, A.; Voss, J.; Nørskov, J. K.; Abild-Pedersen, F. Phys. Rev. B 2014, 89, 115114.
- (26) Jacobsen, C. J. H.; Dahl, S.; Clausen, B. S.; Bahn, S.; Logadottir, A.; Nørskov, J. K. J. Am. Chem. Soc. 2001, 123, 8404–8405.
- (27) Andersson, M. P.; Bligaard, T.; Kustov, A.; Larsen, K. E.; Greeley, J.; Johannessen, T.; Christensen, C. H.; Nørskov, J. K. J. Catal. **2006**, 239, 501–506.
- (28) Greeley, J.; Stephens, I. E. L.; Bondarenko, A. S.; Johansson, T. P.; Hansen, H. A.; Jaramillo, T. F.; Rossmeisl, J.; Chorkendorff, I.; Nørskov, J. K. Nat. Chem. 2009, 1, 552–556.
- (29) Skulason, E.; Tripkovic, V.; Bjørketun, M. E.; Gudmundsdottir, S.; Karlberg, G.; Rossmeisl, J.; Bligaard, T.; Jonsson, H.; Nørskov, J. K. J. Phys. Chem. C **2010**, 114, 18182–18197.
- (30) Jones, G.; Jakobsen, J. G.; Shim, S. S.; Kleis, J.; Andersson, M. P.; Rossmeisl, J.; Abild-Pedersen, F.; Bligaard, T.; Helveg, S.; Hinnemann, B.; Rostrup-Nielsen, J. R.; Chorkendorff, I.; Sehested, J.; Nørskov, J. K. J. Catal. 2008, 259, 147–160.
- (31) Sehested, J.; Larsen, K. E.; Kustov, A. L.; Frey, A. M.; Johannessen, T.; Bligaard, T.; Andersson, M. P.; Nørskov, J. K.; Christensen, C. H. Top. Catal. 2007, 45, 9–13.
- (32) Siahrostami, S.; Verdaguer-Casadevall, A.; Karamad, M.; Deiana, D.; Malacrida, P.; Wickman, B.;

- Escudero-Escribano, M.; Paoli, E. A.; Frydendal, R.; Hansen, T. W.; Chorkendorff, I.; Stephens, I. E. L.; Rossmeisl, J. *Nat. Mater.* **2013**, *12*, 1137–1143.
- (33) Studt, F.; Sharafutdinov, I.; Abild-Pedersen, F.; Elkjaer, C. F.; Hummelshøj, J. S.; Dahl, S.; Chorkendorff, I.; Nørskov, J. K. Nat. Chem. **2014**, *6*, 320–324.
- (34) Grabow, L. C. ChemCatChem **2012**, 4, 1887–1888.

Graphical TOC Entry

